Simulations of interfacial creep generation for shrink-fitted bimetallic work roll

IOP Conf. Series: Materials Science and Engineering **372** (2018) 012026 doi:10.1088/1757-899X/372/1/012026

Simulations of interfacial creep generation for shrink-fitted bimetallic work roll

H Sakai[1,2], N-A Noda[1], Y Sano[1], Y Takase[1] and G W Zhang[1]

[1]Mechanical Engineering Department, Kyushu Institute of Technology Sensui-Cho 1-1 Tobata-Ku, Kitakyushu-Shi, Fukuoka, Japan

E-mail: q595103h@mail.kyutech.jp

Abstract. The bimetallic work rolls are widely used in the roughing stands of hot rolling stand mills. The rolls are classified into two types: one is a single-solid type, and the other is a shrink-fitted construction type consisting of a sleeve and a shaft. Regarding the assembled rolls consisting of a sleeve and a shaft, the interfacial creep phenomenon can be seen between the shaft and the shrink-fitted sleeve. This interfacial creep phenomenon causes the relative displacement on the interface between the sleeve and the shaft. Although to clarify this creep mechanism is important issues, experimental simulation is very difficult to be conducted. In this paper, the interfacial creep phenomenon is realized by using the elastic finite element method (FEM) analysis. It is found that the interface creep can be regarded as the accumulation of the relative circumferential displacement on the interface of the sleeve and the shaft.

1. Introduction

The bimetallic roll is used at the roughing stands of hot rolling stand mills as shown in figure 1. The bimetallic roll is usually manufactured by using centrifugal casting method. However, so-called assembled rolls are sometimes used for large diameter roll having more than 1000 mm [1] and H-shaped steel rolling rolls [2,3] by connecting a hollow sleeve and shafts due to shrink-fitting. Although the wear and surface roughness soon appear on the roll body, the shaft can be reused in this assembled structure. Furthermore, it is easy to provide high wear resistance property to the sleeve. However, the shrink-fitted structure has some inherent problems such as roll residual bending deformation [4-6], shaft breakage due to fretting cracks and interfacial creep. This creep phenomenon often causes damage to the roll, although few studies are available.

It is known that this creep phenomenon can be regarded as relative slippage as a common phenomenon in rolling bearing [7]. Mainly, two types of slippage is known as the creep phenomenon in the bearing. One is the relative slippage appearing in the same circumferential direction as the bearing rotating direction [8]. The other is the relative slippage appearing in the opposite circumferential direction to the bearing rotating direction [9]. It is also known that one of the relative slippage appearing in the opposite direction is caused by the accumulation of elastic deformation. However, few study is available to realize the creep phenomenon in the numerical simulation that is useful for investigating the detail.

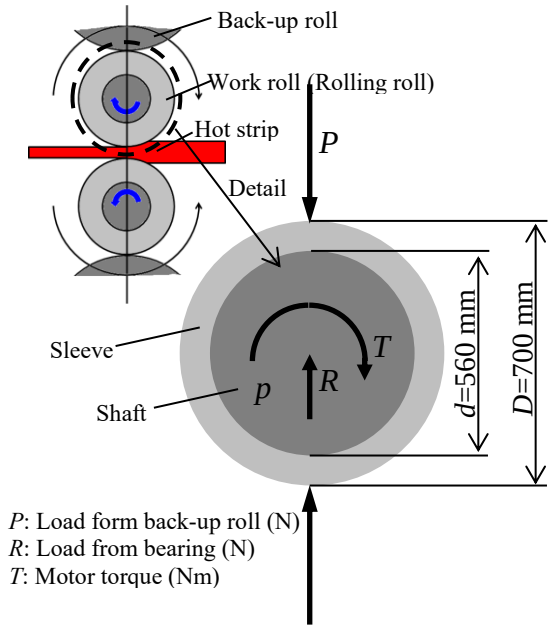

Figure 1. Real rolling roll dimensions with load conditions.

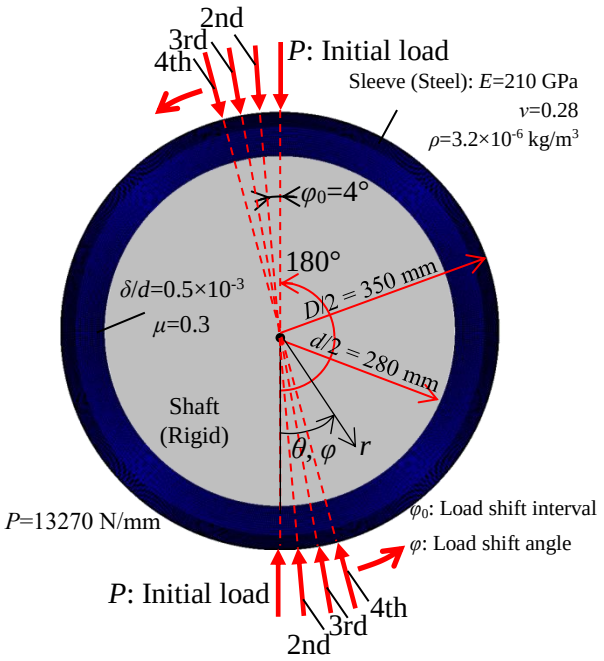

Figure 2. 2D FEM model and boundary conditions.

In this study, therefore, the interfacial creep phenomenon will be realized by using the elastic finite element method (FEM) analysis. Here, elastic deformations will be considered as the most fundamental factors causing the interfacial creep in the rolling roll.

2. FEM modelling to realize the interfacial creep in work roll

In this research, to realize the interfacial creep, a 2D model as shown in figure 2 will be considered. Due to the effect of the elastic deformation on the interfacial creep, the elastic body and rigid body are used in the 2D model. As shown in figure 2, the load from the support roll and the load from the hot strip are applied to this model. The concentrated load from the support roll and the hot strip are balanced, therefore, $R = 0$ in figure 1. The rolling torque from the motor is not considered, therefore, $T = 0$ in figure 1. Additionally, the influence of the thermal expansion of the sleeve on the interfacial creep can be neglected. Therefore we didn't consider it in this paper.

In this study, the interfacial creep will be studied by applying the finite element method (FEM). The FEM is one of the most used numerical modeling techniques, which can be used for many engineering applications conveniently [10-15]. The number of elements of the model used in this study is 46080. Static structural analysis is performed to the roller by using MSC Marc Mentat 2012 with full Newton–Raphson iterative sparse solver of multifrontal method. In this study, a two-dimensional elastic FEM analysis can be applied because the loading condition does not exceed the yielding stress for the steel sleeve.

As shown in figure 2, dimensions of the roller is considered whose outer diameter $D = 700$ mm. Here, the roller consists of steel sleeve and rigid shaft connected by shrink fitting. The shrink fitting ratio is defined as δ/d, where δ is the diameter difference and d is the inner diameter of the sleeve $d = 560$ mm.

As shown in figure 2, the sleeve material is steel whose Young's modulus $E = 210$ GPa, Poisson's ratio $\nu = 0.28$, density $\rho = 3.2\times10^{-6}$ kg/m^3. Also, the friction coefficient between the interface of the sleeve and the shaft is $\mu = 0.3$.

3. Analysis result of the interfacial creep in work roll

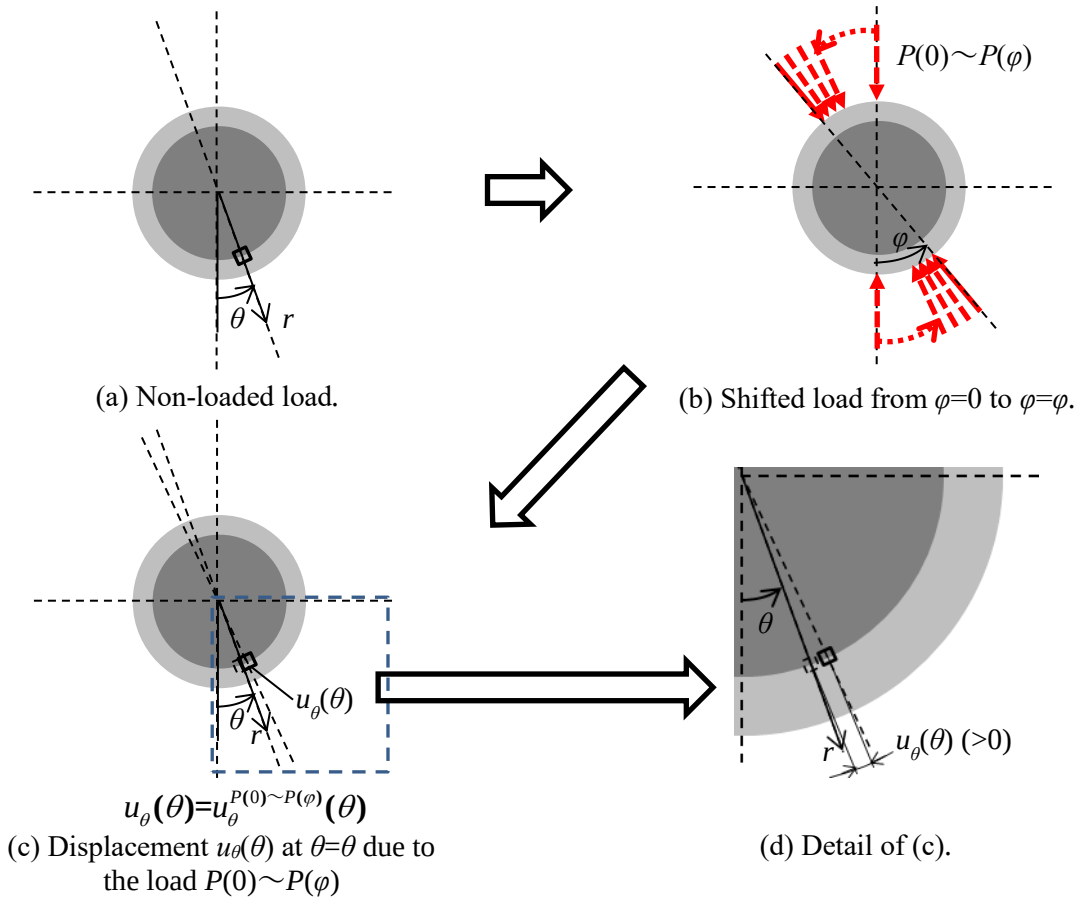

(a) Non-loaded load. (b) Shifted load from φ=0 to φ=φ.

$u_\theta(\theta)=u_\theta^{P(0)\sim P(\varphi)}(\theta)$

(c) Displacement $u_\theta(\theta)$ at θ=θ due to the load $P(0)\sim P(\varphi)$ (d) Detail of (c).

Figure 3. Interfacial displacement $u_\theta^{P(0)\sim P(\varphi)}(\theta)$ at θ due to the shifted

3.1. Determination of the interfacial creep

In order to determine the interfacial creep, the relative circumferential displacements between the interface of the sleeve and shaft will be focused. In this analysis, since the relative circumferential displacement on the interface of the sleeve is equal to the absolute circumferential displacement on the interface of the sleeve because the rigid shaft is fixed. Therefore the circumferential displacement on the interface of the sleeve will be used to determine the interfacial creep. Assume that $u_\theta^{P(0)\sim P(\varphi)}(\theta)$ is the circumferential displacement on the interface of the sleeve. Figure 3 shows the definition of the interfacial displacement $u_\theta^{P(0)\sim P(\varphi)}(\theta)$ under the shifted load from φ = 0 to φ = φ.

To simulate the coming out behaviour, the roll rotation is replaced by the shifted load P [16,17] in the circumferential direction on the fixed roll as shown in figure 2. The roller is under a concentrated to load P = 13700 N/mm. As shown in figure 2, the continuous load shifting can be replaced by discrete load shifting with load shift angle φ_0, which is usually used as a standard discretization numerical analysis. Here, a smaller angle φ_0 provides accurate results but large computational time. Therefore, the optimal angle φ_0 should be discussed by investigating u_θ with varying the shift angle, φ_0 = 12°, φ_0 = 8°, φ_0 = 4°, and φ_0 = 0.25°. Figure 4 shows u_θ focusing on the interfacial creep. Although the result for φ_0 = 12° and φ_0 = 8° are different from others, the result for φ_0 = 0.25° and φ_0 = 4° are almost coincide with each other. Since the effect of discrete load shifting is less than a few percent if $\varphi_0 \leq$ 4°, it may be concluded that the load shifting angle φ_0 = 4° is the most suitable to reduce large calculation time without losing accuracy. In the following calculation the load shift angle φ_0 = 4° will

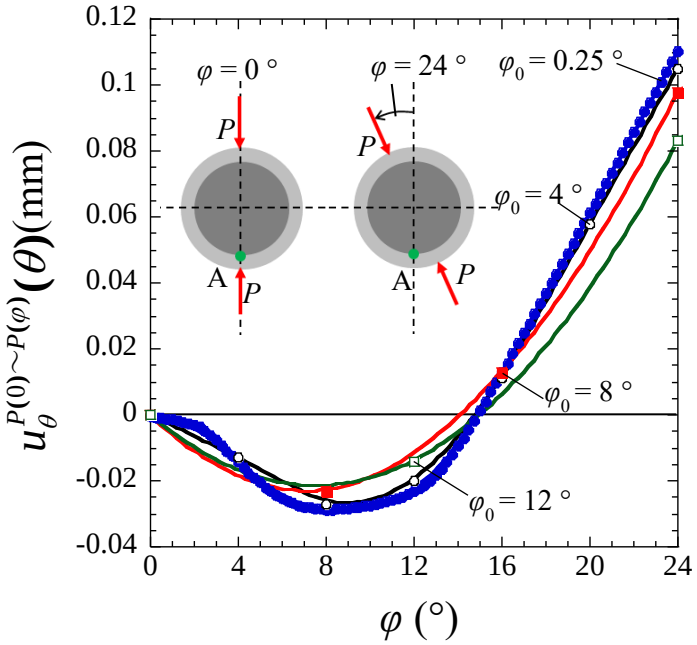

Figure 4. Displacement of the sleeve interface point A when θ_0 = 0.25°, 4°, 8° and 12°.

be used consistently. From figure 4, initially, the displacement of the point A is $u_\theta^{P(0)\sim P(\varphi)} < 0$. This is because the point A is pushed counter-clockwise direction due to the concentrated load on the lower side. Thereafter, the influence of the concentrated load on the upper side is increased, and the point A is pushed clockwise direction. As a result, the displacement of the point A is $u_\theta^{P(0)\sim P(\varphi)} > 0$.

3.2. Displacement on the interface of the sleeve u_θ

Figure 5(a) shows the displacement distribution when the loads are applied at $\varphi = 0$ and $\varphi = \pi$ defined as (a) $u_\theta^{P(0)}(\theta)$. and also (b) $u_\theta^{P(0)\sim P(2\pi/15)}(\theta)$. When the concentrated loads $P(\varphi)$ are applied at $\varphi = 0$ and $\varphi = \pi$ as $P(\varphi) = P(0)$, the deformation is symmetric with respect to the loading points $\varphi = 0$ and the displacement is skew-symmetric. In other words, we have

$$-u_\theta^{P(0)}(-\theta) = u_\theta^{P(0)}(\theta) \ \ (\varphi = 0, 0 \le \theta \le \pi). \tag{1}$$

Figure 5(b) shows the displacement distribution $u_\theta^{P(0)\sim P(2\pi/15)}(\theta)$. In this case, the concentrated loads $P(\varphi)$ are initially applied at $\varphi = 0$ and finally at $\varphi = 2\pi/15$ denoted as $P(\varphi) = P(0) \sim P(2\pi/15)$. In figure 5(b), the deformation is not symmetric anymore with respect to the final loading points $\varphi = 2\pi/15$.

$$-u_\theta^{P(0)\sim P(\varphi)}(-\theta + \varphi) \neq u_\theta^{P(0)\sim P(\varphi)}(\theta + \varphi) \ \ (\varphi > 0, 0 \le \theta \le \pi) \tag{2}$$

Figure 5 also shows the average value of the displacements $u_{\theta,\text{ave.}}^{P(0)}$ and $u_{\theta,\text{ave.}}^{P(2\pi/15)}$. The average displacement along the interface of the sleeve $u_{\theta,\text{ave.}}^{P(0)\sim P(\varphi)}$ is defined in equation (3).

$$u_{\theta,\text{ave.}}^{P(0)\sim P(\varphi)} = \frac{1}{2\pi}\int_0^{2\pi} u_\theta^{P(0)\sim P(\varphi)}(\theta)d\theta \tag{3}$$

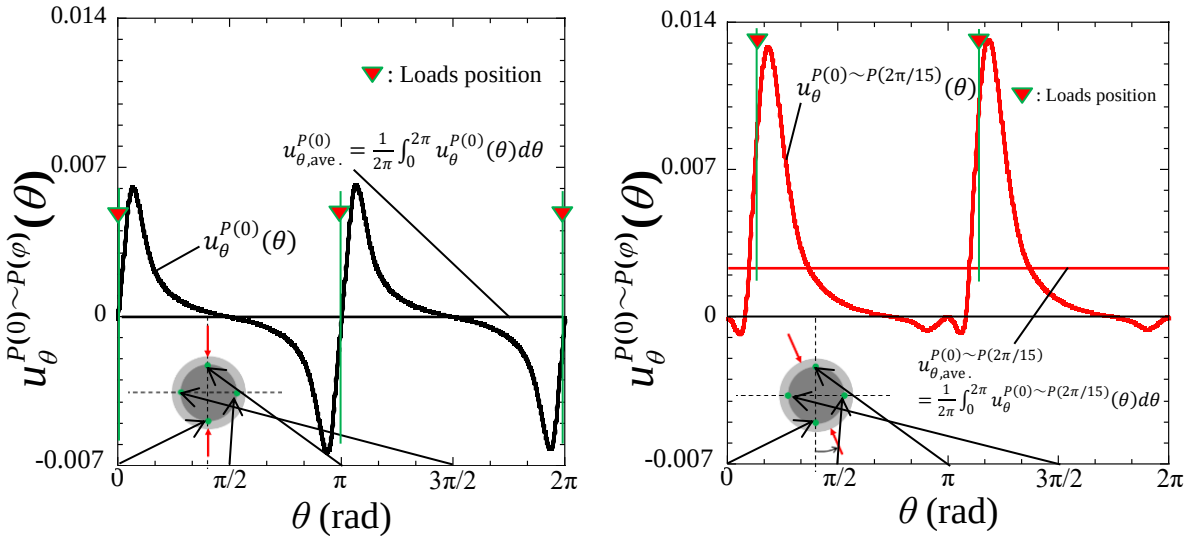

(a) At $P(0)$ (b) At $P(2\pi/15)$

Figure 5. Distribution of displacement of the sleeve interface $u_\theta^{P(0)\sim P(\varphi)}(\theta)$.

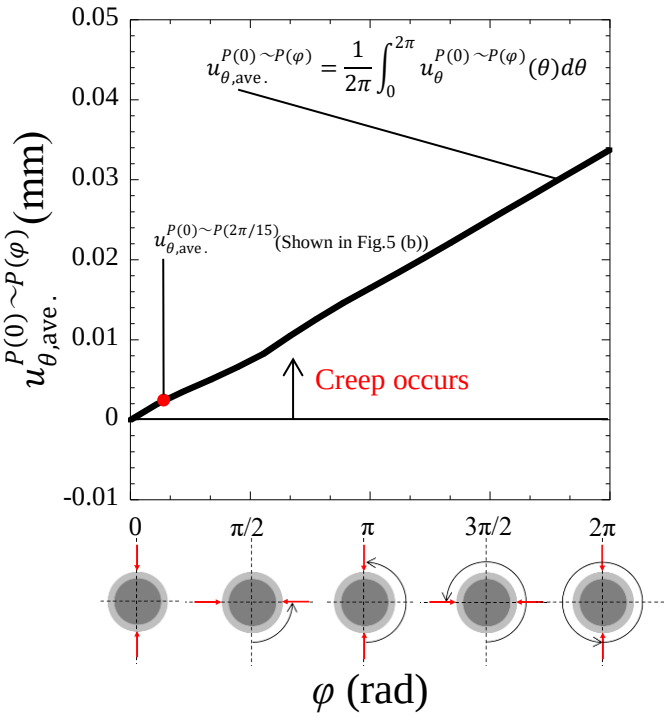

Figure 6. History of average of displacement of the sleeve interface when P is shifted.

Under the initial loads $P(\varphi) = P(0)$, we have $u_{\theta,\text{ave.}}^{P(0)}=0$. This is because the displacement distribution is symmetric. On the other hand, under the shifted loads $P(\varphi) = P(0) \sim P(2\pi/15)$, the average value $u_{\theta,\text{ave.}}^{P(2\pi/15)}$ is not zero anymore because the displacement distribution is not symmetric.

Figure 6 shows the relationship between the average displacement $u_{\theta,\text{ave.}}^{P(0)\sim P(\varphi)}$ and the load shift angle φ. From figure 6, it is found that $u_{\theta,\text{ave.}}^{P(0)\sim P(\varphi)}$ increases with increasing φ. It may be concluded that the interfacial creep occurs as soon as the load shifting starts.

4. Conclusion

- The interface creep phenomenon was realized through quiz-static structural FEM analysis assuming the elastic sleeve and rigid shaft by shifting the load *P* on the fixed 2D work roll.
- The interface creep phenomenon was discussed by focusing on the relative circumferential displacement on the interface of the sleeve and the shaft. The interface creep occurs due to the collapse of the symmetry of the deformation of the sleeve.
- The interface creep can be regarded as the accumulation of the relative circumferential displacement on the interface of the sleeve and the shaft.
- The average of the relative circumferential displacement on the interface of the sleeve and the shaft. $u_{\theta,\text{ave.}}^{P(0)\sim P(\varphi)}$ increases with increasing the load shift angle φ. That means the interfacial creep occurs as soon as the load shifting starts.

References

[1] Shimoda H, Onodera S., Hori K and Dohi O 1966 *Transactions of the Japan Society of Mechanical Engineering* **32** 689-94
[2] Takigawa H, Hashimoto K, Konno G and Uchida S 2003 Current advances in materials and processes *Report of the ISIJ Meeting* **16** 1150-3
[3] Irie T, Takaki K, Tsutsunaga I and Sano Y 1979 *Testu-to-Hagane* **65** 293
[4] Noda N-A, Sano Y, Takase Y, Shimoda Y and Zhang G 2017 *Sosei-toKako* **58** 66-71
[5] Matsunaga E, Sano Y and Nishida S 1997 Current advances in materials and processes *Report of the ISIJ Meeting* **10** 1078
[6] Matsunaga E, Tsuyuki T and Sano Y 1998 Current advances in materials and processes *Report of the ISIJ Meeting* **11** 362
[7] Soda N 1964 *Bearing, Iwanami Shoten* 196-203
[8] Niwa T 2013 *Ntn Technical Review* **81** 100-3
[9] Murata J and Onizuka T 2004 *Koyo Engineering Journal* **166** 41-7
[10] Miyazaki T, Noda N-A, Ren F, Wang Z, Sano Y and Iida K 2017 *Int J Adhes Adhes.* **77** 118-37
[11] Noda N-A, Miyazaki T, Li R, Uchikoba T and Sano Y 2015b *Int J Adhes Adhes.* **61** 46-64
[12] Noda N-A, Uchikoba T, Ueno M, Sano Y, Iida K, Wang Z and Wang G 2015c *ISIJ International* **55** 2624-30
[13] Wang Z, Noda N-A, Ueno M and Sano Y 2016 *Steel Research International* **88** doi: 10.1002/srin.201600353
[14] Noda N-A, Shen Y, Takaki R, Akagi D, Ikeda T, Sano Y and Takase Y 2017 *Theoretical and Applied Fracture Mechanics* **90** 218–27
[15] Noda N-A, Chen X, Sano Y, Wahab M A, Maruyama H and Fujisawa R 2016 *Materials & Design* **96** 476-89
[16] Noda N-A, Suryadi D, Kumasaki S, Sano Y and Takase Y 2015 *Engineering Failure Analysis* **57** 219-35
[17] Noda N-A, Xu Y, Suryadi D, Sano Y and Takase Y 2016 *Journal of ISIJ International* **56** 303-10